Supplementary Material:
Cerebral blood flow rates in recent great apes are greater than in *Australopithecus* species that had equal or larger brains

Computational approaches to evaluate blood flow rate from foramen size

This study uses a new, empirical approach to calculate internal carotid artery (ICA) blood flow rate from the radius of the carotid canal. So it is worthwhile to compare this "empirical equation" with the previous one based on the Poiseuille-derived "shear stress equation". The techniques used to measure the canal size (CT scans, microphotographs and impression casting) are comparable, and a sensitivity analysis of the shear stress equation reveals reasonable accuracy (Qiaohui Hu et al. MS submitted). However, there are two assumptions that weaken the foramen technique and use of the shear stress equation: the arterial wall thickness-to-lumen radius ratio is assumed a constant (Assumption 1) and the scaling of wall shear stress is calculated from the body mass of the animal (Assumption 2).

Assumption 1: The arterial wall thickness-to-lumen radius ratio being a constant is reasonable. Larger arteries develop thicker walls because average wall cross-sectional stress is normalized according to the Principle of Laplace that requires the wall thickness to increase in proportion to blood pressure and the radius of the vessel [1, 2]. Central mean arterial blood pressure is practically independent of body mass in mammals the size of primates [3]. The thickness of large arterial walls increases mainly by adding more elastic layers in the tunica media such that the wall stress is roughly constant, for example, the aorta of a rat has ~8 media layers while a aorta of a human has ~60 layers, each layer opposing similar stresses and normalizing overall wall stress [4]. However, the value of the ratio for the ICA (w = 0.40), used originally [5] and subsequently was not derived from any human ICA. Instead, it was derived from one value of 0.40 in the canine ICA [6], one value of 0.40 in the human common carotid artery (CCA) [7] and an ignored value of 0.36 in the rat posterior communicating artery [8]. The present investigation sought more studies of the wall thickness-to-lumen radius ratio for the human ICA and CCA, eventually finding 14 studies and obtaining a more exact value of w = 0.30.

Assumption 2: The shear stress equation is derived from hydrodynamic theory based on the Poiseuille-Hagen equation: $\dot{Q} = (\Delta P\ \pi\ r_i^4)/(4\ L\ \eta)$, where $\dot{Q}$ is the flow rate of blood ($cm^3\ s^{-1}$) of given viscosity (η; dyne s cm^{-2}), in response to a pressure difference (ΔP; dyne cm^{-2}) along a vessel of known length (L; cm) and internal known radius (r_i; cm). The shear stress equation eliminates ΔP and L and replaces them with a variable that accounts for wall shear stress (τ; dyne cm^{-2}): $\dot{Q} = (\tau\ \pi\ r_i^3)/(4\ \eta)$ [9]. While ΔP is nearly impossible to evaluate on short real vessels, evaluating τ is also difficult to assess without knowing the velocity profile within the vessel. Although once thought to be a constant within the circulatory system regardless of species and artery size, shear stress is not a

constant, but decreases in larger vessels in a non-linear way [10]. Shear stress decreases in individually named arteries with increasing body mass [10-13], and allometric exponents must be found empirically. Published data for ICA lumen radius and flow rate in two species (humans and rats) in relation to body mass (M_b; g) yielded the original empirical equation, $\tau = 167\ M_b^{-0.20}$ [5], which was used subsequently in several studies of primates [5, 14-17]. Our equation was justly criticized for the low sample size and low predictive value [18]. Another problem with the evaluation of wall shear stress is that there is no obvious reason why it should be functionally related to body mass and not blood vessel size alone. Finally, the flow regimes in large arteries may not conform to Poiseuille flow theory, that is, in proportion to radius cubed, as the shear stress equation assumes. Because of these problems, we sought to find the relationship between blood flow rate and arterial lumen size directly and empirically, without reliance on theory, hydrodynamic equations, or calculation of wall shear stress. Recent imaging studies supplied 57 data points for blood flow rate and artery radius in seven cephalic arteries (common carotid, internal carotid, vertebral, basilar, anterior cerebral, middle cerebral and posterior cerebral arteries) in six genera of resting mammals (*Mus*, *Rattus*, *Oryctolagus*, *Canus*, *Homo*, *Equus*) [10]. The data result in a power equation, $\dot{Q} = 155\ r_i^{2.49}$, which we call the "empirical equation" to distinguish it from the "shear stress equation". The empirical equation can calculate blood flow rates from any cephalic foramen and the results compared with calculated values from the shear stress equation. The range of lumen radius covered by the empirical equation is 0.02 – 0.5 cm, which includes the range of measured radii of all haplorhine primates included in this study and the literature (from *Tarsius* sp., $r_i = 0.02$ cm, to *Homo sapiens*, $r_i = 0.24$ cm). This permits an independent re-evaluation of the allometric relationships among extant primates and fossil hominin species.

ICA blood flow calculated with the shear stress and empirical equations

The major determinant of $\dot{Q}_{ICA}$ is arterial lumen radius, because it is raised to the power of 3.0 in the shear stress equation and 2.49 in the empirical equation. Therefore a reduction in the wall thickness-to-lumen radius ratio from 0.40 to 0.30 results in a 25% increase in $\dot{Q}_{ICA}$ in hominins (Fig. S2). Because wall shear stress is lower in larger arteries [10-13], it is lower in the same named arteries in larger animals, which tends to reduce $\dot{Q}_{ICA}$ calculated with the shear stress equation in animals with larger brains. Thus the effect of the wall shear stress factor is to counterbalance the cubic exponent of lumen radius in the shear stress equation to some extent. However, the compensation is not complete. For full compensation, the scaling exponent of wall shear stress with body mass would need to be -0.51, not -0.20. (2.49 - 3.0 = -0.51). Therefore, we expect a lower exponent when using the empirical equation compared to the shear stress equation. However, when the revised wall thickness-to-lumen radius ratio and empirical equation are applied to the $\dot{Q}_{ICA}$ hominin data, there is no significant difference in exponent ($F_{2, 30} = 0.062$; $P = 0.94$), but a significant increase elevation ($F_{2, 32} = 3.53$; $P = 0.04$) (Fig. S2).

The shear stress equation and w = 0.40 was used to calculate Q_{ICA} in primates [17]. The scaling equation from their tabled data is not significantly different from the empirical equation and w = 0.30, either in exponent ($F_{1, 48}$ = 0.034; P = 0.85) or elevation ($F_{1, 49}$ = 1.431; P = 0.24), but there is a slight improvement in the coefficient of determination.

The scaling of $\dot{Q}_{ICA}$ on endocranial volume in haplorhine primates produces an exponent of approximately 1.0 regardless of whether we use the shear stress equation or new empirical equation (Fig. S3), ICA foramen size from two separate studies (Fig. S4), or regional tissue volumes (Fig. 3). This exponent is very high compared to the exponent of 0.75 expected from "Kleiber's Law" for whole body metabolic rate and body mass or the actual exponent, which is significantly lower [19]. Cardiac output in resting mammals scales with an exponent higher than basal metabolic rate, approximately 0.80 [20, 21], and the exponents are 0.80 for the femoral artery, 0.74 for the infrarenal aorta and 0.80 for the common carotid artery [10]. All of these are significantly lower than the exponent of $\dot{Q}_{ICA}$ in haplorhine primates. We conclude that the high exponent represents an unusually high rate of perfusion to the cognitive parts of the haplorhine brain.

Total brain blood flow calculated with the shear stress and empirical equations

This study focuses on the ICA, but it is now possible to apply the empirical equation to the radius of the vertebral artery (VA) that passes through the transverse foramen of the cervical vertebrae. With the best available information, Boyer and Harrington [17] have estimated that the VA lumen radius averages 51% of the foramen radius in nine mammal species. This value is equivalent to an effective wall thickness-to-lumen radius ratio of w = 0.96, although in this case the "wall" is not only the arterial wall but also a large surrounding venous plexus. The veins are negligible in the carotid canal, so the ratio for the ICA is much lower, w = 0.30. Using Boyer and Harrington's tabled values of lumen radii for the VA and ICA, we can use the empirical equation to estimate $\dot{Q}_{VA}$, $\dot{Q}_{ICA}$ and $\dot{Q}_{TOTAL}$ for haplorhine primates (Fig. S5). We see significantly different exponents for $\dot{Q}_{VA}$ and $\dot{Q}_{ICA}$. The VA and ICA supply equally in haplorhines with brains smaller than 15 ml, but the role of the VA progressively diminishes until it supplies about 26% of total perfusion in a 1400 ml human brain. This corresponds well to the fraction measured in imaging studies of humans [22-27]. The exponent for $\dot{Q}_{TOTAL}$ in haplorhines is 0.95±0.06 when using the empirical equation (Fig. S5) and 0.87±0.06 when using Boyer and Harrington's data calculated with the shear stress equation and their assumptions of effective wall thickness [17]. The equations are marginally not significantly different in exponent ($F_{1, 44}$ = 3.585; P = 0.06), but significantly different in elevation ($F_{1, 45}$ = 0.695; P = 0.41). Interestingly, the exponent of total flow for all 49 species of euarchontans is 0.95 calculated with their protocol and 1.04 with the empirical equation. The equations for these regressions are significantly different in exponent ($F_{1, 94}$ = 6.394; P = 0.013), and the $\dot{Q}_{TOTAL}$ below an V_{br} of 55 ml are significantly lower with the empirical equation. In either case, there is a greater than expected total perfusion in larger brains.

Roles of the internal carotid arteries (ICA) and vertebral arteries (VA) in total brain perfusion in haplorhine primates

The entire brain is supplied by both the ICAs and VAs in haplorhine primates. However, unlike the ICAs that fill the carotid foramina, the VAs run through transverse foramina of the cervical vertebrae accompanied by substantial veins that are part of the spinal venous plexus [28, 29]. In humans, for example, the lumen of the vertebral artery occupies only 38% of the transverse foramen area of cervical vertebra C3 [30]. Venous blood from the brains of erect rhesus monkeys flows almost entirely in the venous plexus, with almost none going through the jugular veins [31, 32]. After passing through the cervical vertebrae, the VAs enter the skull through the foramen magnum with the spinal cord and other vessels, which does not inform us about their size.

Nevertheless, Boyer and Harrington [17] determined the relationship between VA lumen radius and transverse foramen radius and evaluated the contribution of the VAs to total blood flow rate, using the shear stress equation. There is an increasing role of $\dot{Q}_{ICA}$, and a decreasing role of $\dot{Q}_{VA}$, in determining overall $\dot{Q}_{TOTAL}$, as V_{br} increases in haplorhine primates. This is evident in the converging scaling regressions for $\dot{Q}_{TOTAL}$ ($\propto V_{br}^{0.87}$) and $\dot{Q}_{ICA}$ ($\propto V_{br}^{0.98}$). Because $\dot{Q}_{TOTAL} \approx \dot{Q}_{ICA} + \dot{Q}_{VA}$, it is apparent that $\dot{Q}_{VA}$ must be approximately proportional to $V_{br}^{0.77}$. According to these relationships, $\dot{Q}_{ICA}$ accounts for only 34% of total flow in the 3.3 ml brain of *Tarsius*, 59% in the 450 ml brain of *Gorilla* and 67% in the 1400 brain of *Homo sapiens*. Based on foramen radius data presented by Boyer and Harrington [17], the new empirical equation confirms converging regressions, and with similar exponents. The revised haplorhine equations are, $\dot{Q}_{ICA} = 0.0065\ V_{br}^{1.01}$, $\dot{Q}_{VA} = 0.0083\ V_{br}^{0.84}$, and $\dot{Q}_{TOTAL} = 0.0143\ V_{br}^{0.95}$ (Fig. S5).

Roles of the ICAs and VAs in total brain perfusion in hominins

In humans, the ICAs supply approximately 75%, and the VAs only 25%, of total brain perfusion ($\dot{Q}_{TOTAL}$) [22-27]. Although the arteries communicate within the Circle of Willis, the ICAs supply 88% of cerebral flow, and the VAs 12% (unpublished flow data from a meta-analysis of 19 human imaging studies of seven major cephalic arteries by the authors). Thus the ICAs are relied upon for servicing almost all of the cognitive parts of the human brain. The VAs supply mainly the upper spinal cord, brainstem and cerebellum.

Unfortunately, we cannot yet evaluate $\dot{Q}_{VA}$ in fossil hominins, because the foramina that the VAs flowed through have not been measured. However, because $\dot{Q}_{TOTAL} \approx \dot{Q}_{ICA} + \dot{Q}_{VA}$, we can ask what the exponent of $\dot{Q}_{VA}$ on V_{br} would be in hominins, if we know that $\dot{Q}_{ICA} = 0.00028\ V_{br}^{1.41}$. Assuming that V_{br} varies between 300 and 1400 ml in hominins, $\dot{Q}_{ICA}$ is 75% of $\dot{Q}_{TOTAL}$ in the 1400 ml human brain, and $\dot{Q}_{TOTAL} \propto V_{br}^{0.95}$ (as it is in haplorhines), then the scaling of $\dot{Q}_{VA}$ can be estimated. The analysis is not as simple as adding or subtracting exponents, because allometric power equations deal precisely with factors, but not terms. Therefore power equations for $\dot{Q}_{TOTAL}$ and $\dot{Q}_{ICA}$ will not result in a power equation for $\dot{Q}_{VA}$, but it will be close.

Here we start the model with the hominin $\dot{Q}_{ICA}$ equation $\dot{Q}_{ICA} = 0.00028\ V_{br}^{1.41}$ and force the power equation for $\dot{Q}_{TOTAL}$ through a point 4/3 times the value of $\dot{Q}_{ICA}$ when V_{br} is 1400 ml for the human brain. We assume arbitrarily a scaling exponent of 0.95 for $\dot{Q}_{TOTAL}$, because that is the exponent for haplorhine primates according to Boyer and Harrington [17]. This defines the allometric equation for total brain perfusion: $\dot{Q}_{TOTAL} = 0.01047\ V_{br}^{0.95}$. $\dot{Q}_{VA}$ is then calculated as the difference $\dot{Q}_{TOTAL} - \dot{Q}_{ICA}$ and plotted (Fig. S6). The equation for this result is described exactly as a polynomial, $\dot{Q}_{VA} = 1.8 \times 10^{-6}\ V_{br}^2 + 3.98 \times 10^{-3}\ V_{br} + 0.486$. The best fit power equation is, $\dot{Q}_{VA} = 0.872\ V_{br}^{0.36}$ ($R^2 = 0.87$). The model shows that if $\dot{Q}_{TOTAL}$ is assumed proportional to $V_{br}^{0.86}$, then $\dot{Q}_{VA}$ scales as $V_{br}^{0.22}$. If $\dot{Q}_{TOTAL}$ is assumed proportional to $V_{br}^{0.73}$, then $\dot{Q}_{VA}$ scales as $V_{br}^{0.00}$.

A scaling exponent of 0.36 for $\dot{Q}_{VA}$ would require the VA lumen radius to scale as $V_{br}^{0.14}$ (0.14 is 0.36 divided by 2.49, which is the exponent of VA lumen radius in the empirical equation). The exponent 0.14 is less than half of the isometric exponent of 0.33. In other words, to achieve the 1.41 exponent for hominin $\dot{Q}_{ICA}$, the radius of the VA would have to shrink, not absolutely, but relative to the size of the brain. This is doubtful, and becomes even more doubtful if we assume that $\dot{Q}_{TOTAL} \propto V_{br}^{0.86}$, as assumed for mammals in general. We hypothesize that, if $\dot{Q}_{VA} \propto V_{br}^{0.84}$ in hominins (as it is in haplorhines), $\dot{Q}_{TOTAL}$ would be approximately proportional to $V_{br}^{1.22}$, a strongly hyperallometric relationship, similar to the hyperallometric scaling of $\dot{Q}_{ICA}$.

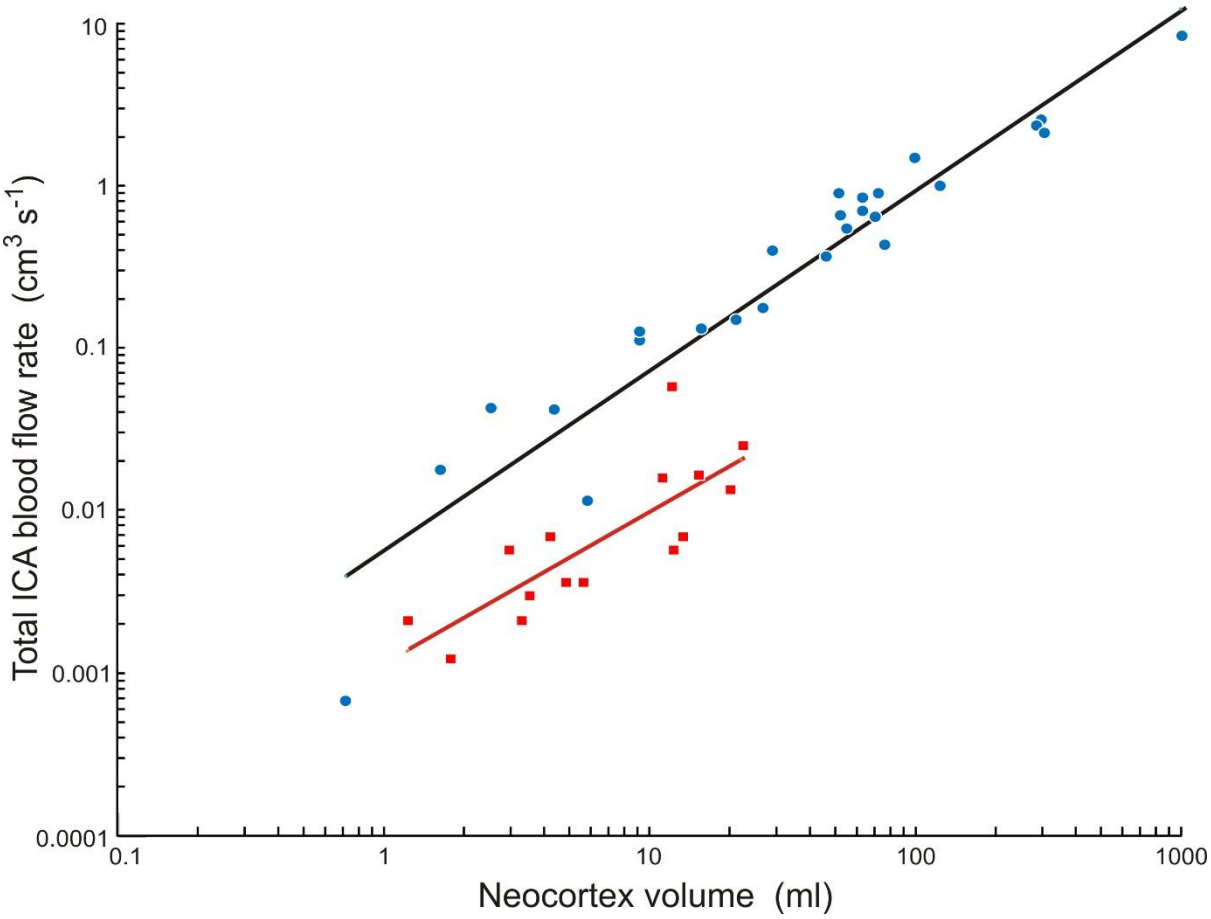

Figure S1. Relationship between total blood flow rate of both ICAs ($\dot{Q}_{ICA}$) and neocortex volume (V_{neo}) in 26 species of haplorhine primates (blue circles) and 15 species of strepsirrhine primates (red squares). Blood flow rates are calculated with the "empirical equation" and w = 0.30 from foramen sizes listed in Seymour et al (2015) [5] and Boyer and Harrington (2019) [17], and neocortical volumes are from dataset 2 in Miller et al. (2019) [33]. The equations are, $\dot{Q}_{ICA} = 0.0062\ V_{neo}^{1.12\pm0.15\ CI}$ ($R^2 = 0.91$) for haplorhines and $\dot{Q}_{ICA} = 0.0012\ V_{neo}^{0.96\pm0.42\ CI}$ ($R^2 = 0.66$) for strepsirrhines. See Table S5 for data.

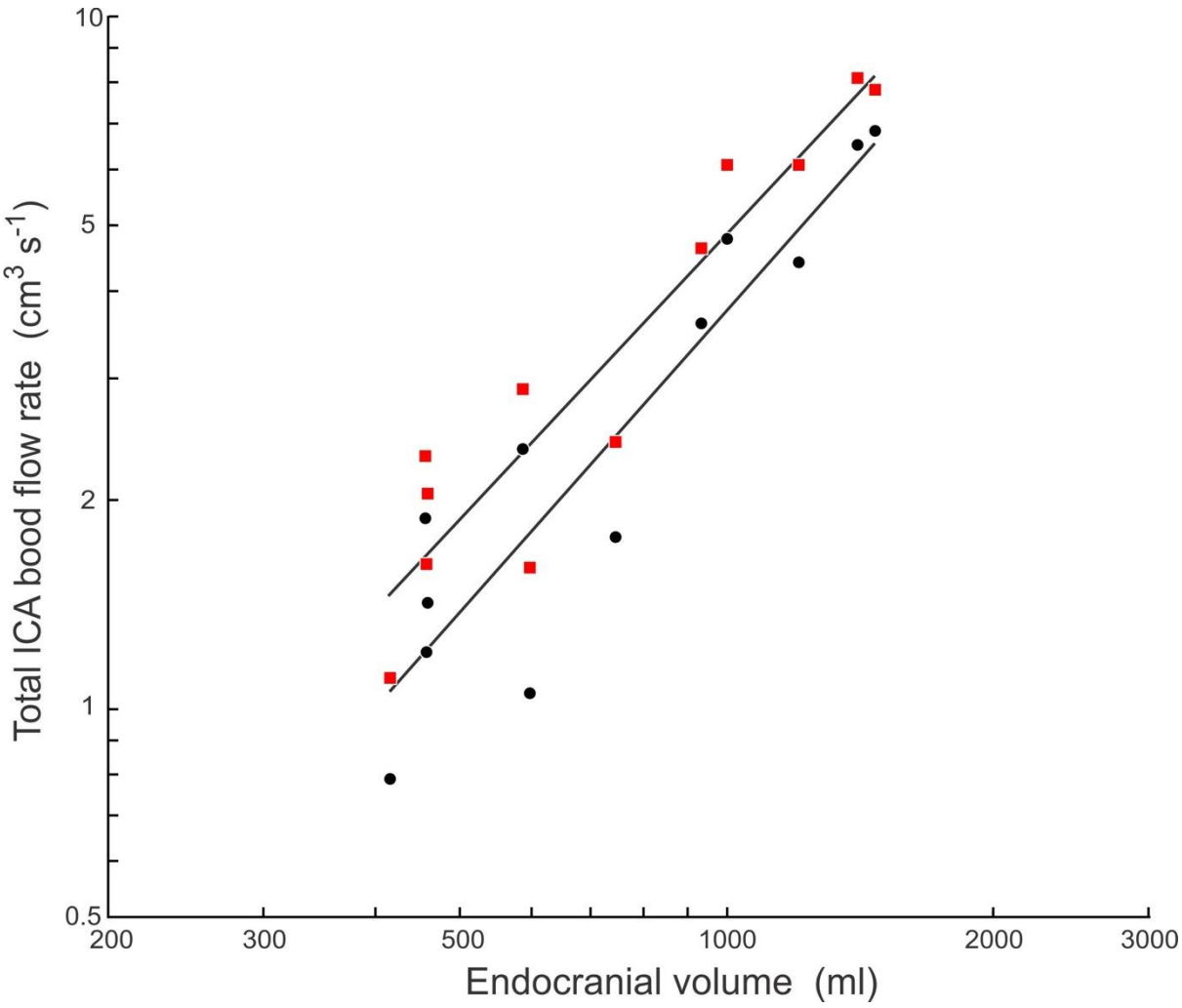

Fig. S2. Comparison of total blood flow rate of both ICAs ($\dot{Q}_{ICA}$) as a function of endocranial volume (V_{br}) in 11 hominin species (Early and Late *H. erectus* are given individual points) calculated from ICA foramen size according to the shear stress equation and assuming w = 0.40 (black circles), and calculated according to the new "empirical equation" and assuming w = 0.30 (red squares). The equations are, $\dot{Q}_{ICA} = 0.000170\ V_{br}^{1.45}$ and $\dot{Q}_{ICA} = 0.000373\ V_{br}^{1.37}$ respectively. ICA foramen data are from Seymour et al. (2017) [15] and do not include *Ardipithecus ramidus*.

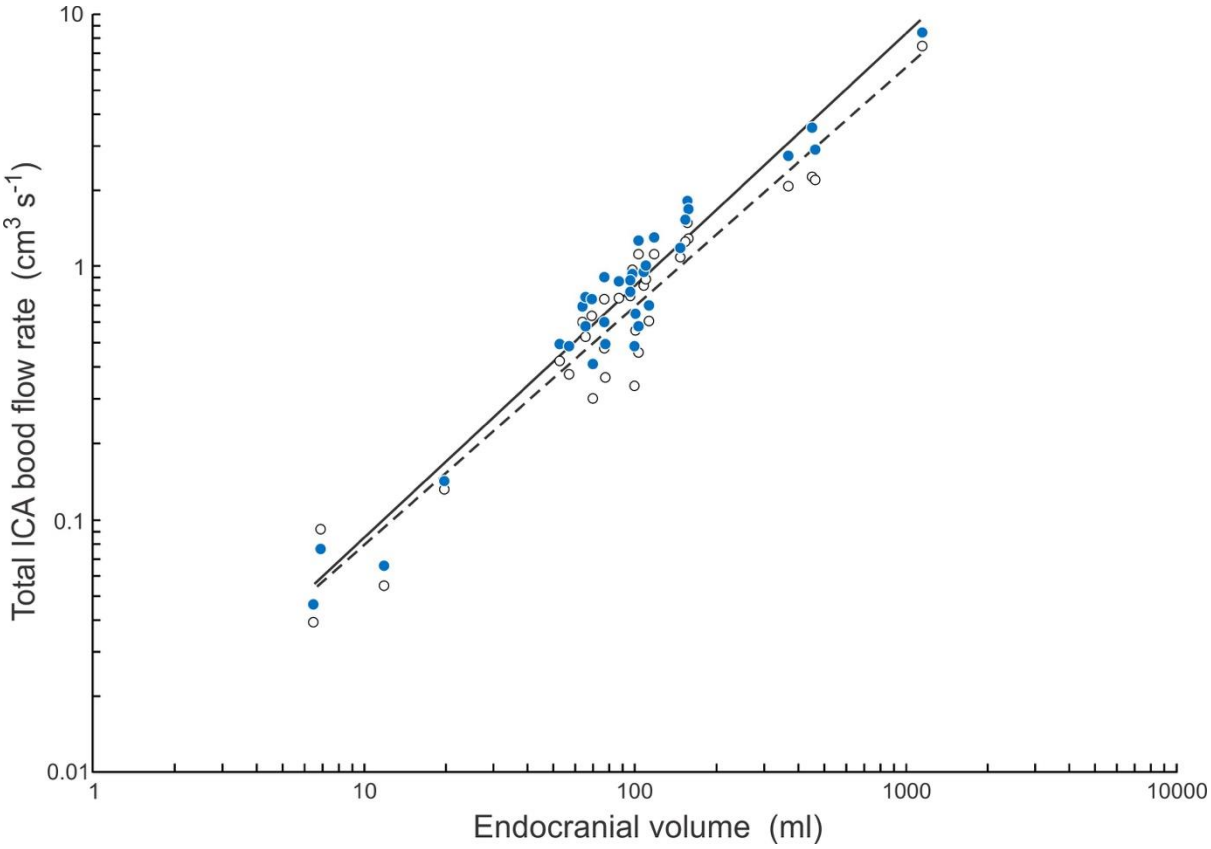

Fig. S3. Comparison of total blood flow rate of both ICAs ($\dot{Q}_{ICA}$) as a function of endocranial volume (V_{br}) in 34 haplorhine species calculated from ICA foramen size. Results from the "empirical equation" and assuming w = 0.30 (blue circles) are compared to results from the shear stress equation and assuming w = 0.40 (open circles). The equations are $\dot{Q}_{ICA} = 0.0084\ V_{br}^{1.00}$ and $\dot{Q}_{ICA} = 0.0088\ V_{br}^{0.95}$, respectively. ICA foramen data are from Seymour et al. (2015) [5].

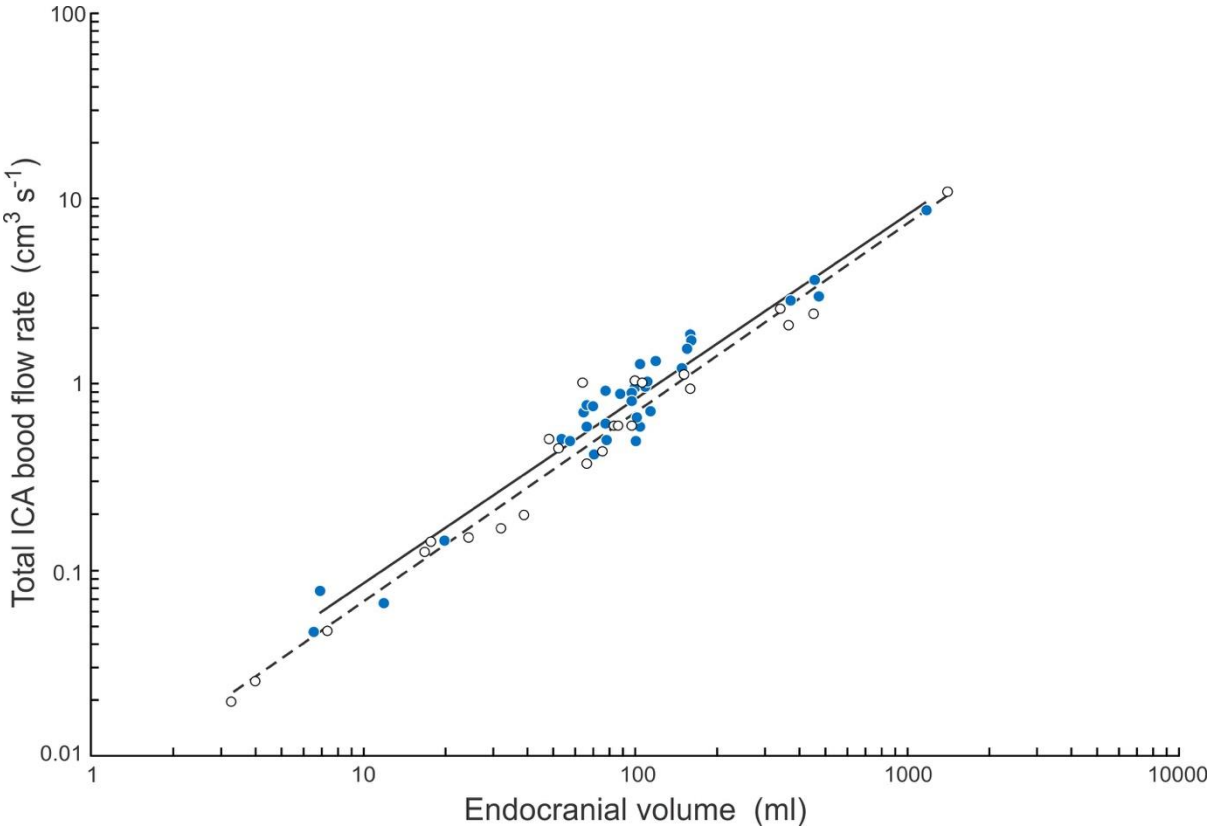

Fig. S4. Total blood flow rate of both ICAs ($\dot{Q}_{ICA}$) as a function of endocranial volume (V_{br}) in haplorhine primates calculated from ICA foramen radius according to the "empirical equation" and assuming w = 0.30. Foramen radius data are derived from 34 species measured by Seymour et al. (2015) [5] (blue circles) and 24 species measured by Boyer and Harrington (2019) [17] (unfilled circles). The equations are, $\dot{Q}_{ICA} = 0.0084\ V_{br}^{1.00}$ and $\dot{Q}_{ICA} = 0.0065\ V_{br}^{1.01}$, respectively.

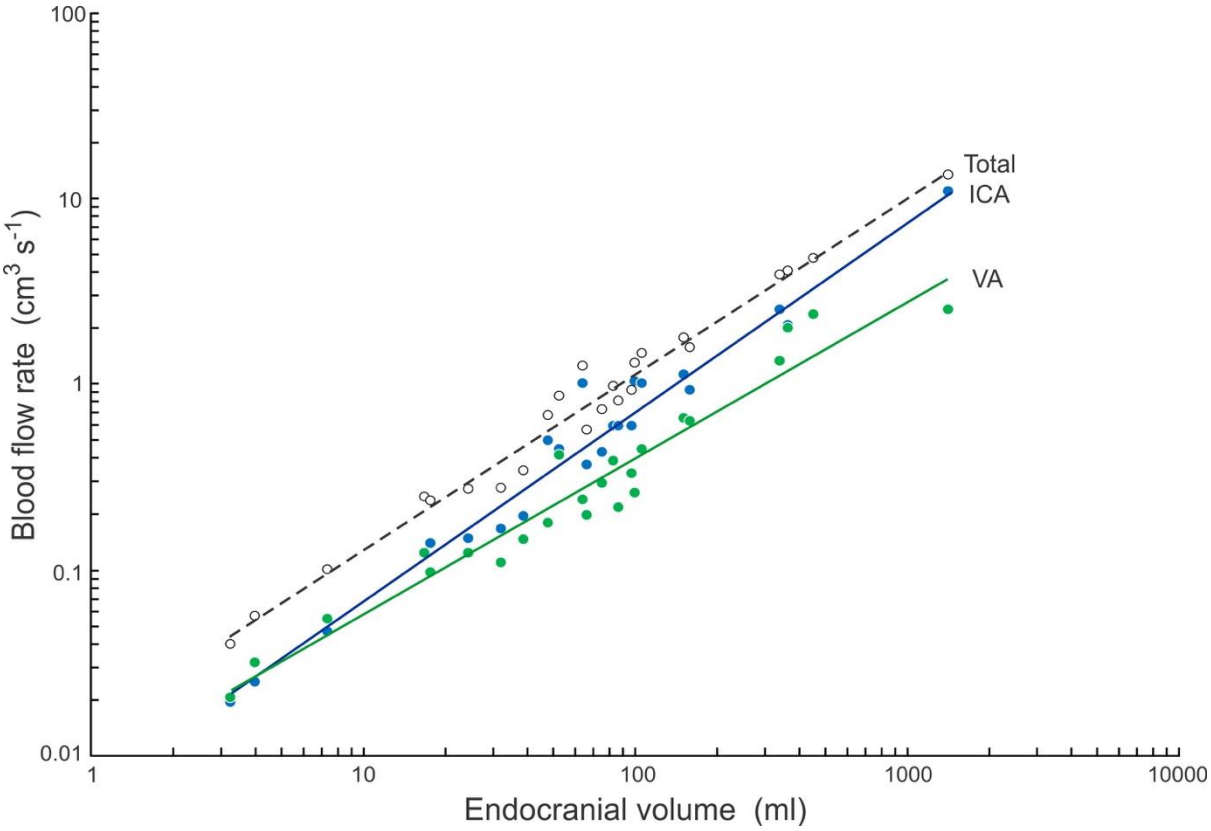

Fig. S5. Blood flow rates of the paired ICAs ($\dot{Q}_{ICA}$), paired vertebral arteries ($\dot{Q}_{VA}$), and the sum of these ($\dot{Q}_{TOTAL}$) plotted as a function of endocranial volume (V_{br}) in 24 haplorhine species calculated from foramen radius according to the "empirical equation" and assuming w = 0.30 for the ICA and w = 0.96 for the VA. Data are derived from foramen radius measured by Boyer and Harrington (2019) [17]. The equations are, $\dot{Q}_{ICA} = 0.0065\ V_{br}^{1.01}$, $\dot{Q}_{VA} = 0.0083\ V_{br}^{0.84}$, and $\dot{Q}_{TOTAL} = 0.0143\ V_{br}^{0.95}$, respectively.

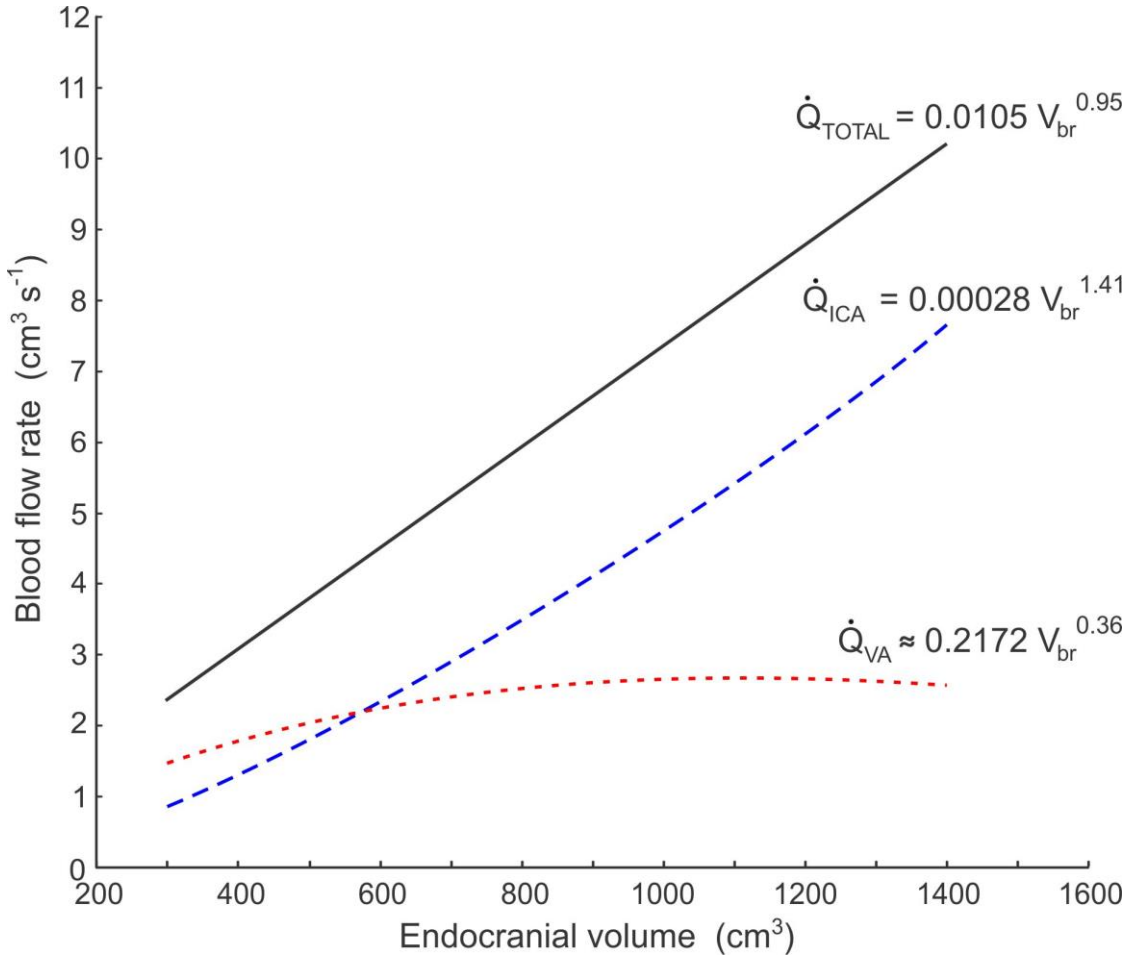

Fig. S6. Model of allometric scaling of hominin brain blood flow rate in relation to endocranial volume (V_{br}). Power equations describe the lines for total brain blood flow rate ($\dot{Q}_{TOTAL}$), which is the sum of blood flow rate in the internal carotid arteries ($\dot{Q}_{ICA}$) and vertebral arteries ($\dot{Q}_{VA}$). The model procedure is described in the Supplementary material text.

Table S1. Literature data for dimensions of the internal carotid artery (ICA), carotid canal and common carotid artery (CCA) in humans.

Study	Method	Artery/canal	Outer radius (mm)	Lumen radius (mm)	Wall thickness (mm)	Wall-lumen ratio	Notes
Sommer et al. 2010	*In vitro*	ICA	3.17	2.56	0.61	0.24	
Watase et al. 2018	MRI	ICA	4.30	3.40	0.90	0.26	
Saam et al. 2009	MRI	ICA	3.98	3.33	0.64	0.19	
Cibis et al. 2016	MRI	ICA	4.52	3.23	1.29	0.40	
Qiao et al. 2016	MRI	ICA	4.82	3.81	1.01	0.26	
Somesh et al. 2014	Manual	Carotid canal	3.60	2.39	1.21	0.51	1
Calguner et al. 1997	Manual	Carotid canal	2.79	2.39	0.40	0.17	1
Naidoo et al. 2017	Manual	Carotid canal	3.23	2.39	0.84	0.35	1
Berlis et al. 1992	Manual	Carotid canal	3.38	2.39	0.99	0.41	1
Aoun et al. 2013	Manual	Carotid canal	3.10	2.39	0.71	0.30	1
Saba et al. 2013	MDCTA	CCA	4.55	3.29	1.26	0.38	2
Saba et al. 2008	MDCTA	CCA	4.11	3.29	0.82	0.25	2
Saba et al. 2010	MDCTA	CCA	4.20	3.29	0.91	0.28	2
Boussel et al. 2007	MRI	CCA	3.91	3.24	0.67	0.21	

Methods: *In vitro*, direct measurements were from arteries fixed of observed at mean physiological pressure of 13.3 kPa. MRI, Magnetic Resonance Imaging. Manual, Direct measurement of bony canal. MDCTA, Multidetector Computed Tomographic Angiography.

Notes: 1, ICA lumen radius taken as the mean from 13 imaging studies [10]. 2, CCA lumen radius taken as the mean from 6 imaging studies [10].

References to be added from below:

[34-47]

Table S2. Summary data for endocranial volume (V_{br}), internal carotid artery (ICA) foramen radius (r_o) and total blood flow rate of both ICAs ($\dot{Q}_{ICA}$) for hominid skulls. Statistics are 95% confidence intervals.

Species	Number	V_{br}	r_o	$\dot{Q}_{ICA}$
		(ml)	(cm)	($cm^3\ s^{-1}$)
Gorilla beringei	16	482 ± 30	0.223 ± 0.009	3.92 ± 0.44
Gorilla gorilla	13	494 ± 40	0.208 ± 0.020	3.39 ± 0.78
Pongo abelii	12	346 ± 28	0.205 ± 0.012	3.19 ± 0.49
Pongo pygmaeus	20	357 ± 17	0.184 ± 0.010	2.44 ± 0.32
Pan troglodytes	19	377 ± 23	0.197 ± 0.013	2.96 ± 0.47
Pan paniscus	2	300	0.178	2.20
Homo sapiens	24	1325 ± 79	0.271 ± 0.010	6.37 ± 0.59
Australopithecus africanus	8	499 ± 56	0.156 ± 0.008	1.60 ± 0.19
Australopithecus afarensis	3	476 ± 74	0.186 ± 0.020	2.46 ± 0.64

Table S3. Endocranial volume and total blood flow rate of both ICAs ($\dot{Q}_{ICA}$) of haplorhine and hominin primates, calculated according to the "empirical equation" (Seymour et al. 2019) [10] and a wall thickness-to-lumen radius ratio of w = 0.30. Data for endocranial volume and ICA foramen radius are from Seymour et al. (2015, 2016) [5, 14]and Boyer and Harrington (2019) [17], except for *Ardipithecus ramidus* which came from [48, 49].

		Endocranial volume	$\dot{Q}_{ICA}$
Species	Taxon	(ml)	($cm^3\ s^{-1}$)
Alouatta sp.	Haplorhini	53	0.445
Aotus trivirgatus	Haplorhini	17	0.123
Ateles geoffroyi	Haplorhini	107	1.007
Cacajao calvus	Haplorhini	88	0.685
Callicebus moloch	Haplorhini	18	0.139
Callithrix jacchus	Haplorhini	7.0	0.046
Callithrix pygmaea	Haplorhini	5.5	0.051
Cebus capucinus	Haplorhini	67	0.367
Cercopithecus mitis	Haplorhini	71	0.413
Cercopithecus neglectus	Haplorhini	65	0.699
Chiropotes satanas	Haplorhini	48	0.496
Chlorocebus aethiops	Haplorhini	67	0.763
Colobus satanas	Haplorhini	79	0.494
Gorilla gorilla	Haplorhini	458	2.970
Homo sapiens	Haplorhini	1304	9.660
Hylobates lar	Haplorhini	106	0.798
Hylobates syndactylus	Haplorhini	120	1.313
Lagothrix lagotricha	Haplorhini	110	0.957
Leontopithecus rosalia	Haplorhini	12	0.065
Lophocebus albigena	Haplorhini	98	0.739
Macaca fascicularis	Haplorhini	71	0.544
Macaca maura	Haplorhini	105	1.272
Macaca mulatta	Haplorhini	78	0.607
Macaca nemestrina	Haplorhini	112	1.014
Macaca nigra	Haplorhini	150	1.196
Macaca ochreata	Haplorhini	98	0.799
Macaca radiata	Haplorhini	67	0.584
Macaca silenus	Haplorhini	89	0.878
Mandrillus leucophaeus	Haplorhini	160	1.376
Mandrillus sphinx	Haplorhini	161	1.696
Miopithecus talapoin	Haplorhini	39	0.194
Nasalis larvatus	Haplorhini	81	0.750
Pan troglodytes	Haplorhini	409	2.713
Papio anubis	Haplorhini	152	1.118
Papio hamadryas	Haplorhini	157	1.538
Piliocolobus badius	Haplorhini	64	1.007

Pithecia pithecia	Haplorhini	32	0.165
Pongo pygmaeus	Haplorhini	372	2.419
Presbytis melalophos	Haplorhini	71	0.747
Saimiri sciureus	Haplorhini	22	0.145
Semnopithecus entellus	Haplorhini	102	0.488
Tarsius sp.	Haplorhini	3.3	0.019
Trachypithecus obscurus	Haplorhini	105	0.584
Trachypithecus vetulus	Haplorhini	58	0.486
Ardipithecus ramidus	Homininae	315	0.843
Australopithecus afarensis	Homininae	457	2.296
Australopithecus africanus	Homininae	458	1.600
Early *Homo erectus*	Homininae	939	4.588
Late *Homo erectus*	Homininae	1004	6.043
Homo habilis	Homininae	590	2.870
Homo georgicus	Homininae	600	1.583
Homo heidelbergensis	Homininae	1213	6.043
Homo neanderthalensis	Homininae	1413	8.068
Homo rudolfensis	Homininae	752	2.404
Homo sapiens	Homininae	1479	7.759
Homo naledi	Homininae	460	2.026
Homo floresiensis	Homininae	417	1.094

Table S4. Volumes of brain regions of haplorhine primates from Navarrete et al. (2018) [50] and total blood flow rate of both ICAs ($\dot{Q}_{ICA}$) calculated according to the new "empirical equation" and w = 0.30 from ICA foramen radius measured by Seymour et al. (2015) [5] and Boyer and Harrington (2019) [17].

Species		Telencephalon volume (ml)	Grey matter volume (ml)	$\dot{Q}_{ICA}$ ($cm^3\ s^{-1}$)
Cercopithecus mitis	Cercopithecidae	57	36	0.413
Lophocebus albigena	Cercopithecidae	78	48	0.730
Macaca fascicularis	Cercopithecidae	43	27	0.542
Macaca mulatta	Cercopithecidae	73	45	0.607
Macaca nemestrina	Cercopithecidae	78	43	1.014
Macaca nigra	Cercopithecidae	61	34	1.196
Macaca silenus	Cercopithecidae	79	51	0.878
Mandrillus sphinx	Cercopithecidae	104	67	1.696
Papio hamadryas	Cercopithecidae	140	85	1.538
Gorilla gorilla	Hominidae	342	174	2.932
Pan troglodytes	Hominidae	287	173	2.708
Pongo pygmaeus	Hominidae	263	164	2.403
Aotus trivirgatus	Platyrrhini	13	10	0.123
Callithrix jacchus	Platyrrhini	6.0	4.3	0.046
Callithrix pygmaea	Platyrrhini	3.2	2.3	0.046
Lagothrix lagotricha	Platyrrhini	76	48	0.957
Leontopithecus rosalia	Platyrrhini	8.7	6.4	0.065

Table S5. Neocortical volumes and total blood flow rate of both ICAs ($\dot{Q}_{ICA}$) of haplorhine and strepsirrhine primates. Neocortical volumes are from dataset 2 in Miller et al. (2019) [33]. Blood flow rate data are calculated from ICA foramen radius in Seymour et al. (2015) [5] and Boyer and Harrington (2019) [17].

Species	Taxon	Neocortex volume (ml)	$\dot{Q}_{ICA}$ ($cm^3\ s^{-1}$)
Alouatta sp.	Haplorhini	29	0.445
Aotus trivirgatus	Haplorhini	9.2	0.123
Ateles geoffroyi	Haplorhini	73	1.007
Callicebus moloch	Haplorhini	9.1	0.139
Callithrix jacchus	Haplorhini	4.4	0.046
Callithrix pygmaea	Haplorhini	2.5	0.046
Cercopithecus mitis	Haplorhini	46	0.413
Gorilla gorilla	Haplorhini	298	2.932
Homo sapiens	Haplorhini	1002	9.620
Hylobates lar	Haplorhini	63	0.788
Lagothrix lagotricha	Haplorhini	63	0.957
Lophocebus albigena	Haplorhini	71	0.730
Macaca mulatta	Haplorhini	55	0.607
Mandrillus sphinx	Haplorhini	99	1.696
Microcebus murinus	Haplorhini	0.7	0.0007
Miopithecus talapoin	Haplorhini	27	0.194
Nasalis larvatus	Haplorhini	52	0.739
Nycticebus coucang	Haplorhini	5.8	0.012
Pan troglodytes	Haplorhini	282	2.708
Papio anubis	Haplorhini	122	1.118
Piliocolobus badius	Haplorhini	51	1.007
Pithecia pithecia	Haplorhini	21	0.165
Pongo pygmaeus	Haplorhini	306	2.403

Saimiri sciureus	Haplorhini	16	0.145
Semnopithecus entellus	Haplorhini	76	0.488
Tarsius sp.	Haplorhini	1.6	0.019
Avahi laniger	Strepsirrhini	4.8	0.0039
Cheirogaleus major	Strepsirrhini	2.9	0.0061
Cheirogaleus medius	Strepsirrhini	1.2	0.0022
Daubentonia madagascariensis	Strepsirrhini	22	0.028
Eulemur fulvus	Strepsirrhini	12	0.0061
Eulemur mongoz	Strepsirrhini	12	0.063
Galago senegalensis	Strepsirrhini	1.8	0.0013
Indri indri	Strepsirrhini	20	0.015
Lemur catta	Strepsirrhini	11	0.017
Lepilemur sp.	Strepsirrhini	3.3	0.0022
Loris tardigradus	Strepsirrhini	3.5	0.0032
Otolemur crassicaudatus	Strepsirrhini	4.2	0.0075
Perodicticus potto	Strepsirrhini	5.6	0.0039
Propithecus verreauxi	Strepsirrhini	13	0.0075
Varecia sp.	Strepsirrhini	15	0.018

1. Burton A.C. 1965 *Physiology and Biophysics of the Circulation*. Chicago, Year Book Medical Publishers Incorporated; 217 p.
2. Caro C.G., Pedley T.J., Schroter R.C., Seed W.A. 2012 *The Mechanics of the Circulation*. Cambridge, Cambridge University Press.
3. White C.R., Seymour R.S. 2014 The role of gravity in the evolution of mammalian blood pressure. *Evolution* **68**, 901-908. (doi:10.1111/evo.12298).
4. Wolinsky H., Glagov S. 1967 A lamellar unit of aortic medial structure and function in mammals. *Circulation Research* **20**, 99-111.
5. Seymour R.S., Angove S.E., Snelling E.P., Cassey P. 2015 Scaling of cerebral blood perfusion in primates and marsupials. *Journal of Experimental Biology* **218**, 2631-2640. (doi:10.1242/jeb.124826).
6. Orsi A.M., Domeniconi R.F., Artoni S.M.B., Filho J.G. 2006 Carotid arteries in the dog: Structure and histophysiology. *International Journal of Morphology* **24**, 239-244.

7. Skilton M.R., Boussel L., Bonnet F., Bernard S., Douek P.C., Moulin P., Serusclat A. 2011 Carotid intima-media and adventitial thickening: Comparison of new and established ultrasound and magnetic resonance imaging techniques. *Atherosclerosis* **215**, 405-410. (doi:10.1016/j.atherosclerosis.2010.12.036).
8. Gules I., Satoh M., Clower B.R., Nanda A., Zhang J.H. 2002 Comparison of three rat models of cerebral vasospasm. *American Journal of Physiology-Heart and Circulatory Physiology* **283**, H2551-H2559. (doi:10.1152/ajpheart.00616.2002).
9. Lehoux S., Tedgui A. 2003 Cellular mechanics and gene expression in blood vessels. *Journal of Biomechanics* **36**, 631-643. (doi:10.1016/S0021-9290(02)00441-4).
10. Seymour R.S., Hu Q., Snelling E.P., White C.R. 2019 Interspecific scaling of blood flow rates and arterial sizes in mammals. *Journal of Experimental Biology* **222**, jeb 199554. (doi:10.1242/jeb.199554).
11. Greve J.M., Les A.S., Tang B.T., Blomme M.T.D., Wilson N.M., Dalman R.L., Pelc N.J., Taylor C.A. 2006 Allometric scaling of wall shear stress from mice to humans: quantification using cine phase-contrast MRI and computational fluid dynamics. *American Journal of Physiology Heart and Circulatory Physiology* **291**, H1700-H1708. (doi:10.1152/ajpheart.00274.2006).
12. Cheng C., Helderman F., Tempel D., Segers D., Hierck B., Poelmann R., van Tol A., Duncker D.J., Robbers-Visser D., Ursem N.T.C., et al. 2007 Large variations in absolute wall shear stress levels within one species and between species. *Atherosclerosis* **195**, 225-235. (doi:10.1016/j.atherosclerosis.2006.11.019).
13. Weinberg P.D., Ethier C.R. 2007 Twenty-fold difference in hemodynamic wall shear stress between murine and human aortas. *Journal of Biomechanics* **40**, 1594-1598. (doi:10.1016/j.jbiomech.2006.07.020).
14. Seymour R.S., Bosiocic V., Snelling E.P. 2016 Fossil skulls reveal that blood flow rate to the brain increased faster than brain volume during human evolution. *Royal Society Open Science* **3**, 160305. (doi:10.1098/rsos.160305).
15. Seymour R.S., Bosiocic V., Snelling E.P. 2017 Correction to 'Fossil skulls reveal that blood flow rate to the brain increased faster than brain volume during human evolution'. *Royal Society Open Science* **4**, 170846. (doi:10.1098/rsos.170846).
16. Seymour R.S., Snelling E.P. 2018 Calculating brain perfusion of primates. *Journal of Human Evolution* **in press**. (doi:10.1016/j.jhevol.2018.06.001).
17. Boyer D.M., Harrington A.R. 2019 New estimates of blood flow rates in the vertebral artery of euarchontans and their implications for encephalic blood flow scaling: A response to Seymour and Snelling (2018). *Journal of Human Evolution* **128**, 93-98. (doi:10.1016/j.jhevol.2018.10.002).
18. Boyer D.M., Harrington A.R. 2018 Scaling of bony canals for encephalic vessels in euarchontans: Implications for the role of the vertebral artery and brain metabolism. *Journal of Human Evolution* **114**, 85-101. (doi:10.1016/j.jhevol.2017.09.003).
19. White C.R., Blackburn T.M., Seymour R.S. 2009 Phylogenetically informed analysis of the allometry of mammalian basal metabolic rate supports neither geometric nor quarter-power scaling. *Evolution* **63**, 2658-2667. (doi:10.1111/j.1558-5646.2009.00747.x).
20. Calder W.A., III. 1996 *Size, Function, and Life History*. 2 ed. Mineola, New York, Dover Publications; 431 p.
21. Holt J.P., Rhode E.A., Holt W.W., Kines H. 1981 Geometric similarity of aorta, venae cavae, and certain of their branches in mammals. *American Journal of Physiology Regulatory, Integrative and Comparative Physiology* **241**, 100-104.
22. Zhao X.X., Zhao M.D., Amin-Hanjani S., Du X.J., Ruland S., Charbel F.T. 2015 Wall shear stress in major cerebral arteries as a function of age and gender--a study of 301 healthy volunteers. *Journal of Neuroimaging* **25**, 403-407. (doi:10.1111/jon.12133).
23. Schöning M., Walter J., Scheel P. 1994 Estimation of cerebral blood flow through color duplex sonography of the carotid and vertebral arteries in healthy adults. *Stroke* **25**, 17-22.

24. Scheel P., Ruge C., Schöning M. 2000 Flow velocity and flow volume measurements in the extracranial carotid and vertebral arteries in healthy adults: reference data and the effects of age. *Ultrasound in Medicine and Biology* **26**, 1261-1266.
25. Ford M.D., Alperin N., Lee S.H., Holdsworth D.W., Steinman D.A. 2005 Characterization of volumetric flow rate waveforms in the normal internal carotid and vertebral arteries. *Physiological Measurement* **26**, 477-488. (doi:10.1088/0967-3334/26/4/013).
26. Sato K., Sadamoto T. 2010 Different blood flow responses to dynamic exercise between internal carotid and vertebral arteries in women. *Journal of Applied Physiology* **109**, 864-869. (doi:10.1152/japplphysiol.01359.2009).
27. Wåhlin A., Ambarki K., Hauksson J., Birgander R., Malm J., Eklund A. 2012 Phase contrast MRI quantification of pulsatile volumes of brain arteries, veins, and cerebrospinal fluids compartments: Repeatability and physiological interactions. *Journal of Magnetic Resonance Imaging* **35**, 1055-1062. (doi:10.1002/jmri.23527).
28. Batson O.V. 1944 Anatomical problems concerned in the study of cerebral blood flow. *Federation Proceedings* **3**, 139-144.
29. Yousry I., Forderreuther S., Moriggl B., Holtmannspotter M., Naidich T.P., Straube A., Yousry T.A. 2001 Cervical MR imaging in postural headache: MR signs and pathophysiological implications. *American Journal of Neuroradiology* **22**, 1239-1250.
30. Kim C., Lee S.H., Park S.S., Kim B.J., Ryu W.S., Kim C.K., Oh M.Y., Chung J.W., Yoon B.W. 2012 A quantitative comparison of the vertebral artery and transverse foramen using CT angiography. *Journal of Clinical Neurology* **8**, 259-264. (doi:10.3988/jcn.2012.8.4.259).
31. Epstein H.M., Linde H.W., Crampton A.R., Ciric I.S., Eckenhoff J.E. 1970 The vertebral venous plexus as a major cerebral venous outflow tract. *Anesthesiology* **32**, 332-337.
32. Eckenhoff J.E. 1971 The vertebral venous plexus. *Canadian Anaesthetists Society Journal* **18**, 487-495.
33. Miller I.F., Barton R.A., Nunn C.L. 2019 Quantitative uniqueness of human brain evolution revealed through phylogenetic comparative analysis. *Elife* **8**, e41250. (doi:10.7554/eLife.41250.001).
34. Sommer G., Regitnig P., Költringer L., Holzapfel G.A. 2010 Biaxial mechanical properties of intact and layer-dissected human carotid arteries at physiological and supraphysiological loadings. *American Journal of Physiology (Heart and Circulatory Physiology)* **298**, H898-H912. (doi:10.1152/ajpheart.00378.2009).
35. Watase H., Sun J., Hippe D.S., Balu N., Li F.Y., Zhao X.H., Mani V., Fayad Z.A., Fuster V., Hatsukami T.S., et al. 2018 Carotid artery remodeling is segment specific: An *in vivo* study by vessel wall magnetic resonance imaging. *Arteriosclerosis Thrombosis and Vascular Biology* **38**, 927-934. (doi:10.1161/atvbaha.117.310296).
36. Saam T., Raya J.G., Cyran C.C., Bochmann K., Meimarakis G., Dietrich O., Clevert D.A., Frey U., Yuan C., Hatsukami T.S., et al. 2009 High resolution carotid black-blood 3T MR with parallel imaging and dedicated 4-channel surface coils. *Journal of Cardiovascular Magnetic Resonance* **11**. (doi:10.1186/1532-429x-11-41).
37. Cibis M., Potters W.V., Selwaness M., Gijsen F.J., Franco O.H., Lorza A.M.A., de Bruijne M., Hofman A., van der Lugt A., Nederveen A.J., et al. 2016 Relation between wall shear stress and carotid artery wall thickening MRI versus CFD. *Journal of Biomechanics* **49**, 735-741. (doi:10.1016/j.jbiomech.2016.02.004).
38. Qiao Y., Guallar E., Suri F.K., Liu L., Zhang Y.Y., Anwar Z., Mirbagheri S., Xie Y.J., Nezami N., Intrapiromkul J., et al. 2016 MR imaging measures of intracranial atherosclerosis in a population-based study. *Radiology* **280**, 860-868. (doi:10.1148/radiol.2016151124).
39. Somesh M.S., Sridevi H.B., Murlimanju B.V., Pai S.R. 2014 Morphological and morphometric study of carotid canal in Indian population. *International Journal of Biomedical Research* **5**, 455-460. (doi:10.7439/ijbr).
40. Çalgüner E., Turgut H.B., Gözil R., Tunc E., Sevim A., Keskil S. 1997 Measurements of the carotid canal in skulls from Anatolia. *Acta Anatomica* **158**, 130-132.

41. Naidoo N., Lazarus L., Ajayi N.O., Satyapal K.S. 2017 An anatomical investigation of the carotid canal. *Folia Morphologica* **76**, 289-294. (doi:10.5603/FM.a2016.0060).
42. Berlis A., Putz R., Schumacher M. 1992 Direct and CT measurements of canals and foramina of the skull base. *The British Journal of Radiology*, 653-661.
43. Aoun M.A., Nasr A.Y., Aziz A.M.A. 2013 Morphometric study of the carotid canal. *Life Science Journal* **10**, 2559-2562.
44. Saba L., Sanfilippo R., Montisci R., Suri J.S., Mallarini G. 2013 Carotid artery wall thickness measured using CT: Inter- and intraobserver agreement analysis. *American Journal of Neuroradiology* **34**, E13-E18. (doi:10.3174/ajnr.A2796).
45. Saba L., Sanfilippo R., Pascalis L., Montisci R., Caddeo G., Mallarini G. 2008 Carotid artery wall thickness and ischemic symptoms: evaluation using multi-detector-row CT angiography. *European Radiology* **18**, 1962-1971. (doi:10.1007/s00330-008-0962-5).
46. Saba L., Sanfilippo R., Montisci R., Mallarini G. 2010 Carotid artery wall thickness: comparison between sonography and multi-detector row CT angiography. *Neuroradiology* **52**, 75-82. (doi:10.1007/s00234-009-0589-5).
47. Boussel L., Serusclat A., Skilton M.R., Vincent F., Bernard S., Moulin P., Saloner D., Douek P.D. 2007 The reliability of high resolution MRI in the measurement of early stage carotid wall thickening. *Journal of Cardiovascular Magnetic Resonance* **9**, 771-776.
48. Suwa G., Asfaw B., Kono R.T., Kubo D., Lovejoy C.O., White T.D. 2009 The *Ardipithecus ramidus* skull and its implications for hominid origins. *Science* **326**, 68-68e67. (doi:10.1126/science.1175825).
49. Kimbel W.H., Suwa G., Asfaw B., Rak Y., White T.D. 2014 Ardipithecus ramidus and the evolution of the human cranial base. *Proceedings of the National Academy of Sciences of the United States of America* **111**, 948-953. (doi:10.1073/pnas.1322639111).
50. Navarrete A.F., Blezer E.L.A., Pagnotta M., de Viet E.S.M., Todorov O.S., Lindenfors P., Laland K.N., Reader S.M. 2018 Primate brain anatomy: New volumetric MRI measurements for neuroanatomical studies. *Brain Behavior and Evolution* **91**, 109-117. (doi:10.1159/000488136).